The influence of tumor oxygenation on hypoxia imaging in murine squamous cell carcinoma using [^{64}Cu]Cu-ATSM or [^{18}F]Fluoromisonidazole positron emission tomography

KEN-ICHIRO MATSUMOTO[1], LAWRENCE SZAJEK[2], MURALI C. KRISHNA[1], JOHN A. COOK[1], JURGEN SEIDEL[3], KELLY GRIMES[1], JOANN CARSON[2], ANASTASIA L. SOWERS[1], SEAN ENGLISH[1], MICHAEL V. GREEN[3], STEPHEN L. BACHARACH[3], WILLIAM C. ECKELMAN[2] and JAMES B. MITCHELL[1]

[1]Radiation Biology Branch, Center for Cancer Research, National Cancer Institute, National Institutes of Health; [2]PET Department and [3]Department of Nuclear Medicine, National Institutes of Health Clinical Center, Bethesda, MD, USA

Received December 1, 2006; Accepted January 8, 2007

Abstract. [^{64}Cu]Cu(II)-ATSM (^{64}Cu-ATSM) and [18F]-Fluoromisonidazole (^{18}F-FMiso) tumor binding as assessed by positron emisson topography (PET) was used to determine the responsiveness of each probe to modulation in tumor oxygenation levels in the SCCVII tumor model. Animals bearing the SCCVII tumor were injected with ^{64}Cu-ATSM or ^{18}F-FMiso followed by dynamic small animal PET imaging. Animals were imaged with both agents using different inspired oxygen mixtures (air, 10% oxygen, carbogen) which modulated tumor hypoxia as independently assessed by the hypoxia marker pimonidazole. The extent of hypoxia in the SCCVII tumor as monitored by the pimonidazole hypoxia marker was found to be in the following order: 10% oxygen > air > carbogen. Tumor uptake of ^{64}Cu-ATSM could not be changed if the tumor was oxygenated using carbogen inhalation 90 min post-injection suggesting irreversible cellular uptake of the ^{64}Cu-ATSM complex. A small but significant paradoxical increase in ^{64}Cu-ATSM tumor uptake was observed for animals breathing air or carbogen compared to 10% oxygen. There was a positive trend toward ^{18}F-FMiso tumor uptake as a function of changing hypoxia levels in agreement with the pimonidazole data. ^{64}Cu-ATSM tumor uptake was unable to predictably detect changes in varying amounts of hypoxia when oxygenation levels in SCCVII tumors were modulated. ^{18}F-FMiso tumor uptake was more responsive to changing levels of hypoxia. While the mechanism of nitroimidazole binding to hypoxic cells has been extensively studied, the avid binding of Cu-ATSM to tumors may involve other mechanisms independent of hypoxia that warrant further study.

Correspondence to: Dr James B. Mitchell, Radiation Biology Branch, National Cancer Institute, Bldg. 10, Room B3-B69, 9000 Rockville Pike, Bethesda, MD 20892, USA
E-mail: jbm@helix.nih.gov

Key words: tumor hypoxia, PET, imaging, Cu-ATSM, FMiso

Introduction

Hypoxic regions exist within tumors which may compromise the efficacy of radiotherapy and chemotherapy (1-6). Therefore *a priori* information of tumor hypoxia may be useful in the choice of treatment modalities. Non-invasive imaging methods that can provide spatially resolved qualitative/quantitative pO_2 information are desirable. Nuclear medicine techniques using hypoxia specific tracers (7,8) and PET imaging using hypoxia specific tracers such as ^{18}F-labeled misonidazole (9) and Cu-ATSM are being evaluated for their capability in providing such information (10-14).

Copper complexes of the thiosemicarbazine ligands have been recently identified as agents useful in nuclear medicine to assess hypoxia and blood flow (15). Cu(II)-ATSM is a neutral lipophilic molecule, which is highly membrane permeable and can undergo reduction by cellular reducing equivalents and be converted to [Cu(I)-ATSM]$^-$ (15), which becomes entrapped in cells by virtue of the unit negative charge. The reducing agents for Cu(II)-ATSM were variously identified as complex I of the mitochondrial electron transport chain, NADH cytochrome b5 reductase, NADPH cytochrome P-450 reductase, or intracellular thiols (15). ^{64}Cu(II)-ATSM, unlike the ^{64}Cu(II)-PTSM analog, is di-alkylated and therefore more resistant to reduction except under significant hypoxic conditions (16).

While several thiosemicarbazine ligands bind only Cu(II) but not Cu(I), the cuprous complex dissociates after reduction and released copper is bound to cellular macromolecules (17). However, the Cu(I) complex of ATSM was suggested to be stable and remain intact even under strongly acidic conditions (16) and by virtue of its charge, it is trapped intracellularly when cells are hypoxic. Nitroimidazole agents undergo cellular reduction (7,18,19), and in hypoxic conditions, are irreversibly converted to covalent adducts, ring fragmentation, and side-chain cleavage. However, in the case of Cu(II)-ATSM, two possible situations for the reduced [Cu(I)-ATSM]$^-$ may exist under hypoxic conditions: i) stable [Cu(I)-ATSM]$^-$ complexes generated under hypoxic conditions are restricted to intracellular spaces (16); ii) dissociation of the [Cu(I)-

ATSM]$^-$ complex generated by reduction of the cupric state and the release of Cu(I) which may subsequently be stored in intracellular macromolecules (17). If the former mechanism is operative *in vivo*, subsequent reoxygenation can support oxidation of [Cu(I)-ATSM]$^-$ to Cu(II)-ATSM, which, because of it's neutral charge is once again membrane permeable and can be exported out of cells.

Based on the above considerations, we hypothesized that the initial tumor uptake of Cu(II)-ATSM should decrease if the tumor is subsequently oxygenated. The cell permeable Cu(II)-ATSM is reduced in hypoxic cells to the stable, cell-impermeable [Cu(I)-ATSM]$^-$. Subsequent reoxygenation should oxidize the complex once again to the cell permeable cupric complex [Cu(II)-ATSM], which will be cell permeable resulting in a decrease in image intensity. When a sequence of PET images obtained after ^{64}Cu-ATSM administration are collected from an animal breathing room air (21% O_2) and compared to subsequent PET images when the same animal was switched to breathing carbogen (95%), the difference images may show decreased intensity in regions which become reoxygenated. To test this hypothesis, we carried out PET studies of tumor bearing mice administered with either ^{64}Cu-ATSM or ^{18}F-FMiso when breathing gases with different oxygen content, known to cause changes in tumor pO_2 (20). Additional immunohistochemical studies in the same model were carried out using the hypoxia marker pimonidazole.

Materials and methods

Animals and tumors. Female C3H mice, produced by the National Cancer Institute Animal Production Area (Frederick, MD), were used for this study. The mice were 7-9 weeks of age at the time of experimentation and weighed between 20 and 30 g. Experiments were carried out under a protocol approved by the National Cancer Institute Animal Care and Use Committee, and were in compliance with the Guide for the Care and Use Of Laboratory Animal Resource, (1996) National Research Council. Tumors were grown in the mice by a subcutaneous (s.c.) injection of a single-cell suspension of $2x10^5$ squamous cell carcinoma (SCCVII) cells on the right hind leg to a size of ~1.0 cm diameter 7-10 days after injection. Tumor volumes were determined prior to PET scanning, by measuring three orthogonal diameters using calipers. For all imaging studies ~1-cm diameter tumors were used.

Isotope preparation

$^{64}CuCl_2$ and ^{64}Cu-ATSM. ^{64}Cu ($t_{1/2}$ = 12.7 h) was produced at the NIH by the irradiation of a thin layer of ^{64}Ni (Isoflex, USA) electroplated on a solid gold internal target plate of the CS-30 cyclotron utilizing the nuclear reaction ^{64}Ni(p,n)^{64}Cu and separated from the target material as [^{64}Cu]$CuCl_2$ by anion chromatography as described (21). The preparation of [^{64}Cu]Cu-ATSM followed the procedure of Obata *et al* (22). The specific activity of [^{64}Cu]Cu-ATSM as determined by HPLC was 1.21±0.40 Ci/mmol (EOB).

^{18}F-HF and ^{18}F-FMiso. ^{18}F ($t_{1/2}$ = 109.77 m) was produced at the NIH on a GE PETtrace cyclotron utilizing the ^{18}O(p,n)^{18}F nuclear reaction. ^{18}F-FMiso was prepared from no carrier added [^{18}F]fluoride by a previously described method (23). The specific activity of ^{18}F-FMiso as determined by HPLC was 3600±300 Ci/mmol (EOB).

PET scanner. PET images were obtained with the ATLAS (Advanced Technology Laboratory Animal Scanner), a small animal PET scanner with an axial field-of-view (FOV) of 2 cm, a transverse FOV of 6.8 cm and an aperture of 8 cm (24-26). Image data acquired with the ATLAS PET scanner were reconstructed using a three-dimensional reconstruction algorithm (27).

PET scan experimental conditions. Each mouse was anesthetized with isoflurane (induction 2.0%; maintenance 1.5%) carried by air at 750 ml/min and delivered via a nosepiece. Once anesthesia was established further isoflurane was carried by either air (20.9% oxygen), carbogen (95% oxygen/5% CO_2), or 10% oxygen/90% nitrogen. In order to inject ^{64}Cu-ATSM or ^{18}F-FMiso intravenously (i.v.), a cannula was inserted into the tail vein (30-gauge ½" needle inserted into one end of a 60-cm length of PE10 tubing; IntraMedic Polyethylene, Becton Dickinson and Company, Sparks, MD). IV lines were filled with heparin (100 USP U/ml) prior to cannulation. A bladder catheter (PE10 tubing) was used to collect urine output and a rectal temperature probe (Fiso Fiber Optic Temperature Gauge, GenTek, Norcross, GA) was used to monitor core body temperature. Mice were immobilized in a specialized jig that secured the feet. This jig was inserted into a cylindrical Lucite chamber, fixed with a port for the attachment of thermostat-controlled, warm air circulator (Nikon Model ITC-32, Nikon Inc. Japan) in order to maintain the mouse's core temperature at 37˚C. The entire assembly was fixed to a computer-controlled motorized gantry capable of precisely moving the animal into the scanner. After a core temperature of 37˚C was established, PET image collection was started, and a 100-μl bolus of ^{64}Cu-ATSM (1-4 mCi) or ^{18}F-FMiso (200-400 μCi) in 0.9% saline was injected. Accurate measurements of the injected dose were recorded for each animal imaged.

The first series of studies were designed to test the hypothesis that ^{64}Cu-ATSM trapped in the tumor because of hypoxia might leak out when better oxygenation was provided to the tumor. For this experiment 3 mice were injected with ^{64}Cu-ATSM while breathing air. Dynamic images over the tumor were acquired for 180 min beginning just prior to the injection. At 90 min post-injection, the animals were switched to breathing carbogen. The second series of studies were designed to determine whether tumors took up more ^{64}Cu-ATSM when the animal was injected while breathing air compared to carbogen. Three tumor-bearing animals were injected with ^{64}Cu-ATSM while breathing air and dynamic imaging (beginning just prior to injection) was performed for 120 min (extended to 180 min in one animal). Another 3 mice were injected with ^{64}Cu-ATSM while breathing carbogen, and again dynamically imaged from just prior to injection to 120 min (extended to 180 min for 1 mouse). In addition, ^{64}Cu-ATSM tumor uptake studies were carried out on mice breathing 10% oxygen (used to increase tumor hypoxia). Similar studies were conducted using ^{18}F-FMiso.

To address the problem of mouse-to-mouse variations in tumor uptake, which might mask true changes in tumor uptake when air or carbogen was used, double injection studies were performed. Two mice were injected (^{64}Cu-ATSM) while breathing air and imaged dynamically for ~140 min. Seventy min into imaging, the mouse was switched to carbogen and injected again (15 min after beginning carbogen inhalation). Dynamic imaging was continuous throughout the entire 140 min. Two additional mice were studied in the same way, but began by breathing carbogen, were injected and 70 min later switched to air and injected again. This experiment permitted measuring how much uptake of ATSM occurs in the same tumor in the same mouse as a function of which gas was being administered (and therefore how well oxygenated the tumor was).

Integral blood input functions were determined by continuously collecting blood after injection with ^{64}Cu-ATSM. A catheter was placed in the jugular vein with PE10 tubing and connected to a Harvard pump. Blood was collected in the tubing for 30 min post-injection at a rate of 2 μl/min. After the collection, each end of the tubing was sealed, the tubing was placed in a counting tube, and the sample was counted. Total activity was corrected for decay, activity, and the weight of each respective tumor-bearing animal (air breathing, n=6; carbogen breathing, n=6).

Volumes of interest (VOI) were drawn semi-automatically over the tumors using a three dimensional region growing program from IDL (Research Systems Inc., Boulder, CO), based on a 40% (or in some cases other percentages, as described below) threshold of the maximum counts in a manually drawn crude region around the tumor. Values within the VOI were expressed as relative activity concentration per mCi injected per gram of body weight, unless otherwise specified. All data were corrected for radioactive decay.

Whole body ^{64}Cu-ATSM PET scan fusion with CT. Following some of the tumor scans with ^{64}Cu-ATSM, whole body PET scans were performed. Immediately after whole body PET scans, whole body CT scans (MicroCAT, CTI/ImTek, Inc., Knoxville, TN) were performed. The lucite fixture used for the PET scans was made to also fit the CT scanner, so that the animal could be scanned in the same orientation on both units.

Immunohistochemical assessment of hypoxia. Immunohistochemical analysis of tumor hypoxia was determined using the hypoxia marker, pimonidazole (28). Tumor-bearing mice were placed under conditions identical to the PET imaging studies for the hypoxia marker studies. Animals (n=3 per condition) were anesthetized with isoflurane and placed on a temperature-controlled water circulating pad adjusted to maintain a core body temperature of 37˚C. After equilibration, the isoflurane breathing mixture was carried by air (21% oxygen), carbogen (95% oxygen/5% CO_2), or 10% oxygen/90% nitrogen. After 15 min of breathing the various mixtures, pimonidazole was injected i.p. and the respective isoflurane/oxygen mixtures were continued for 90 min. Following this exposure period, animals were euthanasized, tumors excised, and stored at -70˚C.

Tumor samples embedded with OCT compound (Sakura Finetek, Torrance, CA) were sectioned (6-μm sections) and placed on slides and processed with pimonidazole monoclonal antibody (200 μg/ml, Hydroxyprobe™, Chemicon International, Inc., Temecula, CA) (28). Secondary anti-mouse IgG antibodies conjugated with Alexa Fluor 488 (2 μg/ml, Molecular Probes, Eugene, OR) were incubated for 1 h at room temperature. Sections were exposed to propidium iodide (PI, 50 μg/ml, Sigma, St. Louis, MO) for 2 min. Epifluorescent images were collected on an inverted microscope (Zeiss Axiovertvert 200, Carl Zeiss MicroImaging, Inc., Thornwood, NY) equipped with a mercury light source and CCD camera (Cooke Sensicam, Romulus MI). PI (which stains all nuclei red) and pimonidizole levels were quantified using ImagePro Plus (Mediacybernetics, Silver Spring MD). Images were taken and a histogram map of the grayscale intensities established. A threshold was established which prevented any grayscale intensities below the threshold from being included in the pimonidazole maps. The pimonidazole grayscale map was converted to a binary image for % area determination for each part of the section analyzed (4 per slide examined). Immediately after the pimonidazole image was taken, the microscope spectral filter was changed to detect the PI fluorescence (>600 nm). Again, as with the pimonidazole imaging, grayscale images were obtained and converted to binary maps to obtain the % PI area. The hypoxic fraction was determined by dividing the % area for the pimonidazole labeling divided by the % area of the PI staining. Data are expressed as the mean fluorescence value of four randomly selected regions within a tissue section (n=3 tumors). Data were analyzed using a 2-sided Student's t-test with unequal variances.

Results

To study the distribution of ^{64}Cu-ATSM in the tumor-bearing mouse, PET/CT studies were carried out in air breathing mice. ^{64}Cu-ATSM uptake was observed in the abdomen, tumor-bearing leg, and head region of the animals. To better localize the uptake in the head, whole body CTs were conducted and the CT image was fused with the PET image (Fig. 1). The ^{64}Cu-ATSM uptake in the head region did not appear to be in the brain, but localized to the nasal cavity and/or sinus. The reason for the uptake in this region is unknown.

Dynamic tumor uptake of ^{64}Cu-ATSM as a function of time is shown in Fig. 2. This experiment permitted determination of whether uptake of ^{64}Cu-ATSM in a presumably hypoxic tumor washes out when the animal is made to breath carbogen. The ordinate has units proportional to average activity concentration (decay corrected) in the VOI (30% threshold) surrounding the tumor divided by the dose injected/g of whole body weight. Corrections were made for radioactive decay. As can be seen in the plot (each curve from a different mouse), there was essentially no change in ^{64}Cu-ATSM tumor uptake after carbogen breathing oxygenated the tumor.

Fig. 2 demonstrated that ^{64}Cu-ATSM does not wash out with oxygenation by carbogen breathing. ^{64}Cu-ATSM tumor uptake was next determined when animals were injected while breathing air, compared to animals injected while breathing carbogen as shown in Fig. 3. There was no statistically significant difference between tumor uptake (at 120 min) for tumors injected while breathing air or while breathing carbogen (0.92±0.14 versus 0.97±0.20, p=NS). However,

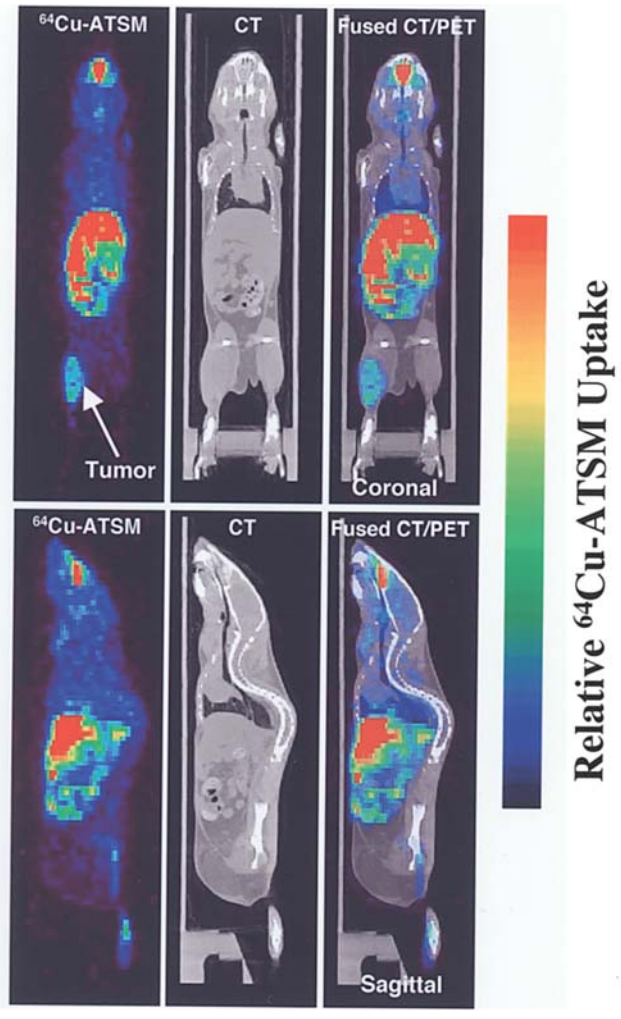

Figure 1. Coronal (top) and sagittal (bottom) whole body scans of a SCCVII tumor-bearing mouse: left, ^{64}Cu-ATSM scans; middle, CT scans; right, fused ^{64}Cu-ATSM/CT scans. Whole body scans revealed uptake of ^{64}Cu-ATSM in the abdomen, tumor-bearing leg, and head region of the animals.

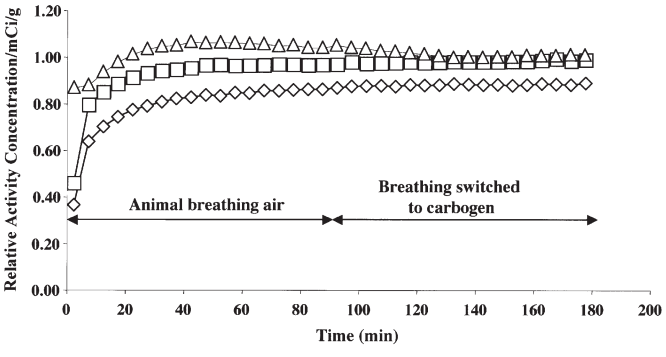

Figure 2. Dynamic tumor uptake of ^{64}Cu-ATSM as a function of time. Tumor-bearing animals breathing air (n=3) were injected with ^{64}Cu-ATSM and tumor uptake followed by small animal PET imaging for 90 min. After 90 min of breathing air the animals were switched to carbogen breathing and the tumor was imaged for an additional 90 min.

there was considerable variation of ^{64}Cu-ATSM total tumor uptake for both air and carbogen breathing animals. This variability might influence the ability to detect air/carbogen differences. To reduce these variations we measured air versus

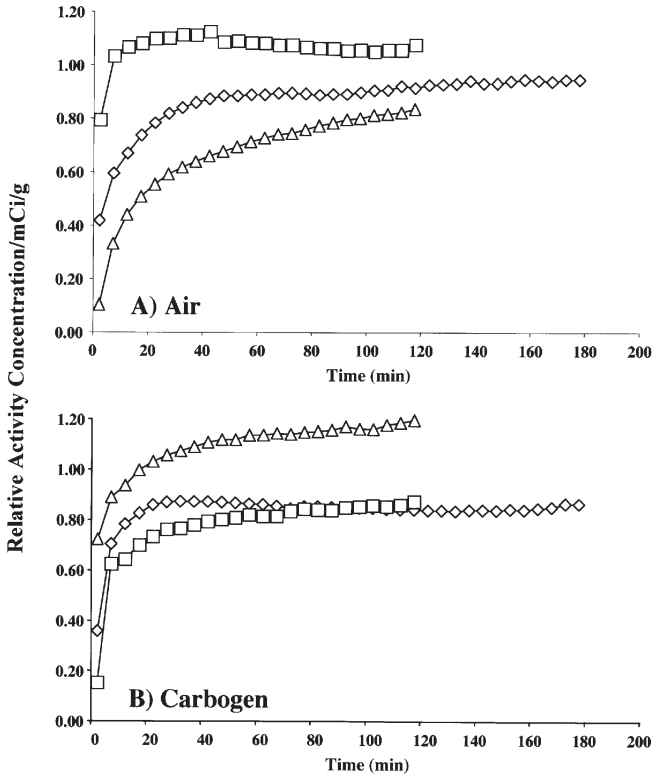

Figure 3. Tumor-bearing animals breathing air (A) or carbogen (B) were injected with ^{64}Cu-ATSM and tumor uptake followed by small animal PET imaging as a function of time. Different symbols denote individual mice.

carbogen ^{64}Cu-ATSM tumor uptake differences in the same tumor bearing animal. These studies utilized 2 separate injections of ^{64}Cu-ATSM in the same animal (60-70 min apart), one while breathing air, one while breathing carbogen (Fig. 4). The second injection is corrected for the residual activity left from the first injection. This correction was performed in the following way: based on the data in Figs. 2 and 3 it was empirically determined that the shape of the tumor time activity curve could be very accurately described by $A^*(1. - \exp(-B^*\text{time}))^*\exp(C^*\text{time})$, for times 10 min post-injection and later. Therefore, the data from 10 to 60 min following each of the first injections in Fig. 4 was fit to this function (solid curves in Fig. 4) for each mouse. This function was then used to subtract residual activity from injection 1 from the data of injection 2. The result of this subtraction is shown in the data from >60 min (i.e. the 2nd injection) in Fig. 4, along with the corrected data (solid curve). Note that the initial activity at the time of second injection does not necessarily start at zero because the injection was not synchronized to the start of a new dynamic image. For the air → carbogen studies (Fig. 4A and B) in both mice carbogen ^{64}Cu-ATSM tumor uptake was greater than that observed when the animal was breathing air. For the reverse condition (carbogen → air, Fig. 4C and D), one animal showed greater ^{64}Cu-ATSM tumor uptake for carbogen (Fig. 4C), while the second animal (Fig. 4D) showed greater tumor uptake while breathing air. Collectively, three of four animals gave a result opposite to that expected, i.e., ^{64}Cu-ATSM tumor uptake would be greater for animals breathing air (more hypoxia compared to when breathing carbogen).

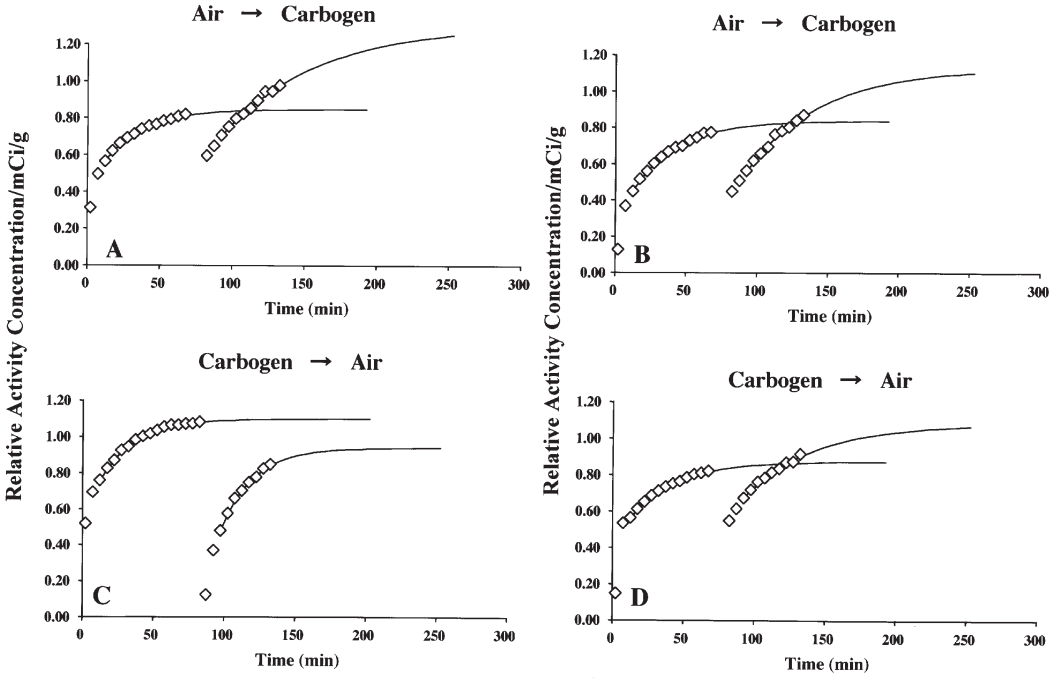

Figure 4. Dynamic tumor uptake of ^{64}Cu-ATSM as a function of time. For these studies animals received an initial injection of ^{64}Cu-ATSM while breathing air (A and B, n=2) and tumor uptake followed by microPET. After 90 min, the breathing mixture was switched to carbogen and 15 min after the carbogen breathing was initiated the animal was re-injected with a second injection of ^{64}Cu-ATSM followed by tumor uptake assessment by small animal PET imaging. C and D show the reverse sequence, carbogen → air (n=2). Extrapolated data from the first injection were subtracted from the second injection.

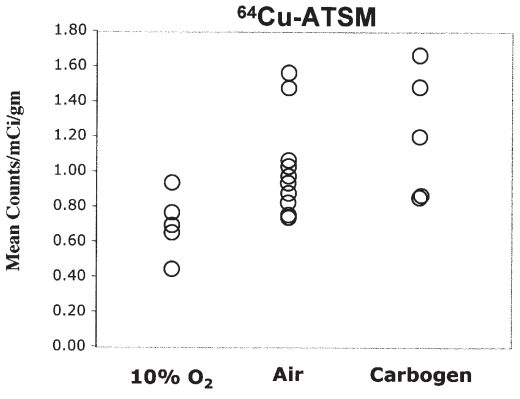

Figure 5. Mean tumor uptake of ^{64}Cu-ATSM for the various breathing mixtures evaluated. Each symbol represents a different tumor-bearing mouse.

The arterial input function could change depending on which gas the mouse was breathing. Because of the challenges involved in estimating the arterial input function from images of an animal as small as a mouse, integrals of the arterial input functions were obtained by continuously collecting venous blood after injection with ^{64}Cu-ATSM. Blood was collected 30 min post-injection of ^{64}Cu-ATSM from tumor-bearing mice (matched to the mice in the imaging study for weight and tumor size). After the collection the entire sample was counted. Total activity was corrected for decay, activity, and the weight of each respective tumor-bearing animal (air breathing, n=6; carbogen breathing, n=6). Aside from any first pass extraction in the lung, this integral should equal the integral of arterial blood. The mean integral blood input, expressed as CPM/μCi/g for air and carbogen breathing animals, was 25.5±6.7 and 24.6±8.5, respectively (p=NS). Thus, no correction to the tumor ^{64}Cu-ATSM uptake was made.

Additional ^{64}Cu-ATSM tumor uptake studies were conducted for animals breathing 10% oxygen, which should make the tumor even more hypoxic. The mean tumor uptake of ^{64}Cu-ATSM when the animal was breathing 10% oxygen (n=5), 21% oxygen (air) (n=10), or carbogen (95% oxygen) (n=5) is shown in Fig. 5. Where mice were studied with two injections, only the data from the first injection is used in Fig. 5. Mean ^{64}Cu-ATSM tumor uptake in the tumors was 0.701±0.177 (SD), 1.02±0.28 and 1.21±0.36 for the 10%, 21%, and 95% oxygen mice, respectively. Both the 21% and 95% oxygen tumor uptake were significantly higher than the 10% oxygen uptake ($p<0.04$, ($p<0.02$, respectively). The 21% versus 95% oxygen uptakes were not significantly different.

The results using ^{64}Cu-ATSM indicated that altered tumor oxygenation did not affect ^{64}Cu-ATSM tumor uptake. Since this result was unexpected, we conducted another series of experiments using a different hypoxia marker ^{18}F-FMiso. Transaxial images of different mice injected ^{64}Cu-ATSM or ^{18}F-FMiso while breathing air are shown in Fig. 6. ^{64}Cu-ATSM tumor uptake was more uniform than ^{18}F-FMiso, which exhibited hot regions and colder regions in the tumor. Hot regions were analyzed separately by 3D region growing taking all pixels with ≥90% of the maximum value within the tumor. When the ^{18}F-FMiso images were analyzed for binding as a function of time by considering either the hot-spots (regions of high binding) or the entire tumor (Fig. 7), the following observations were noted. First, the binding in the whole tumor reached a maximum within ~10 min after injection when the animals were breathing air or carbogen.

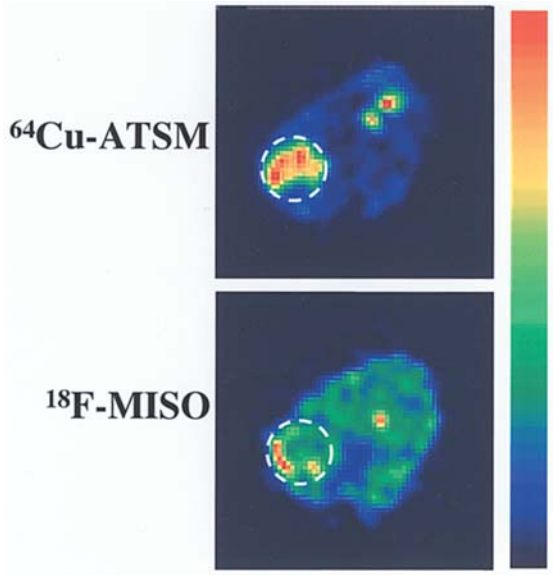

Figure 6. Representative axial images of tumor-bearing mice breathing air and injected with ^{64}Cu-ATSM (top) or ^{18}F-FMiso (bottom). Dashed circle shows approximate tumor location.

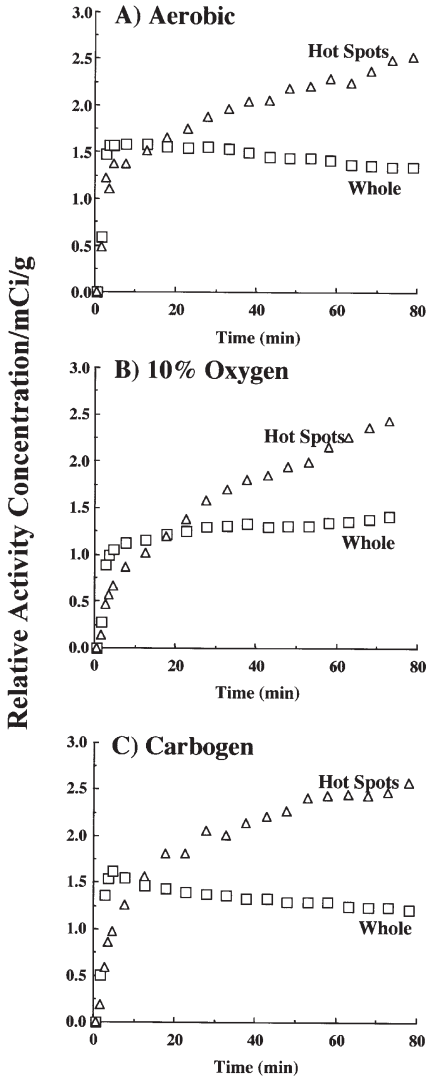

Figure 7. Dynamic tumor uptake of ^{18}F-FMiso as a function of time for animals breathing air (A), 10% oxygen (B), or carbogen (C).

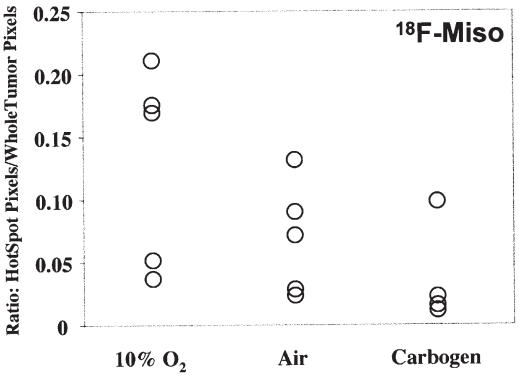

Figure 8. Summary of ^{18}F-FMiso tumor uptake for the various breathing mixtures evaluated expressed as a ratio of the 'hot' pixels in the tumor to the whole tumor pixels. Each symbol represents a different tumor-bearing mouse.

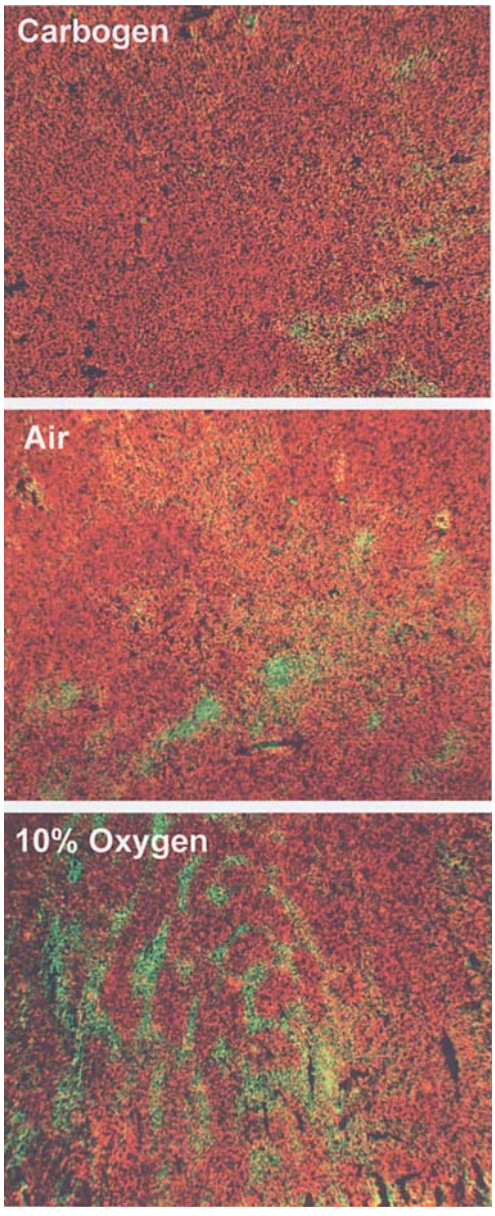

Figure 9. Representative photomicrographs of SCCVII tumor sections taken from animals treated with hypoxia marker pimonidazole and exposed to varying breathing mixtures; carbogen (top), air (middle), or 10% oxygen (bottom). Green color is positive for pimonidazole; red color is propidium iodide, which stains all cell nuclei.

However, when the animal was breathing 10% oxygen the binding gradually increased until the end of the scan. Second, when the hot-spots were examined as a function of time they behaved very differently than the tumor as a whole. For the hot tumor regions a steady increase in uptake was noted in all the conditions of oxygen content in breathing gas tested. We examined whether the fraction of the tumor, which had high uptake differed depending on the oxygen concentration that was administered. The fractional volume of hot pixels versus oxygenation (Fig. 8) showed the binding to be in the following increasing order: 10% oxygen > air > carbogen (0.130±0.079, 0.0696±0.044 and 0.0378±0.04, respectively). However, none of these values were significantly different from any other.

Assessment of tumor oxygenation status was conducted using the hypoxia marker pimonidazole. Representative photomicrographs are shown in Fig. 9 of pimonidazole tumor cell binding (green) for animals breathing different oxygen mixtures. The hypoxia index (ratio of pimonidazole fluorescence divided by PI fluorescence) for air, carbogen, and 10% oxygen breathing was 18.7±7.1 (SD), 7.9±1.3 ($p<0.11$), and 36.0±7.0 ($p<0.04$), respectively.

Discussion

The initial hypothesis of this study proposed that tumor uptake of ^{64}Cu-ATSM would decrease if the tumor were oxygenated. This hypothesis was based on two assumptions. The first assumption was that tumor hypoxia can be decreased if a tumor-bearing animal is administered carbogen. The SCCVII tumor used in the present study is known to be quite hypoxic; however, carbogen breathing increases tumor oxygenation as measured by oxygen electrodes and functional OMRI studies in our laboratory (20). Additionally, pimonidazole staining studies indicated that carbogen breathing increased oxygenation in the SCCVII tumor (Fig. 9). The second assumption was that the cell permeable ^{64}Cu-ATSM complex would be reduced initially in hypoxic tumor cells to the stable cell-impermeable [Cu(I)-ATSM]$^-$ and that subsequent reoxygenation of hypoxic tumor cells should oxidize the complex back to ^{64}Cu-ATSM resulting in a decrease in tumor uptake (16). Data presented in Fig. 2 show that we were unable to obtain data to support the hypothesis. The tumor uptake of ^{64}Cu-ATSM was clearly unchanged when the tumor-bearing animal was switched to carbogen breathing. [^{64}Cu(I)-ATSM]$^-$ is no longer stable as a complex and Cu(I) can be released and sequestered by cellular proteins in the intracellular milieu in agreement with the suggestion of Lewis *et al* (29).

While ^{64}Cu-ATSM binds to tumor avidly, binding to the abdomen and nasal cavity was observed (Fig. 1). ^{64}Cu-ATSM has recently been proposed to target tumor hypoxia for therapeutic radiation treatment (11,30). That ^{64}Cu-ATSM will bind to aerobic tissues is consistent with the data of Lewis *et al*, whose *in vitro* studies showed that the uptake of ^{64}Cu-ATSM in cells under aerobic conditions was approximately 40% (10). Given the more effective cell killing by radiation under aerobic as opposed to hypoxic conditions, caution should be exercised in considering ^{64}Cu-ATSM for tumor treatment with regard to normal tissue toxicity.

There was considerable variability in ^{64}Cu-ATSM tumor uptake within each experimental group, despite careful attention to using animals of the same age, weight, tumor size, normalized ^{64}Cu-ATSM dose, and keeping experimental conditions the same. To minimize this variability, experiments were conducted where the same mouse was injected twice, once while breathing air and then switched to carbogen and injected again, and the reverse sequence (Fig. 4). With appropriate corrections (subtracting the tumor uptake from the first injection and projecting the tumor uptake of the second injection), only 1 of 4 animals exhibited the expected oxygen-dependent ^{64}Cu-ATSM tumor uptake. Considering all of the studies conducted with ^{64}Cu-ATSM separately (Figs. 2-4), we were unable to demonstrate a consistent relationship between tumor oxygenation and ^{64}Cu-ATSM uptake. However, when we combined all air, carbogen and 10% oxygen studies (Fig. 5) a small but significant paradoxical increase in ^{64}Cu-ATSM uptake was found between 10% and 95% oxygen ($p<0.02$) and between 10% and 21% oxygen ($p<0.04$). In both cases ^{64}Cu-ATSM uptake increased with increasing tumor oxygen concentrations. This finding was unexpected and the reasons for the discrepancy between this study and published reports (29) with ^{64}Cu-ATSM are not clear. Lewis *et al*, reported an oxygen dependency of ^{61}Cu-ATSM tumor uptake of rat 9L gliosarcoma based on tumor oxygenation modulated by treatment with hydralazine (to induce more hypoxia) and breathing 100% oxygen (29). Time-activity curves for ^{61}Cu-ATSM tumor uptake were conducted for 27 min post-injection. Hydralazine treatment resulted in slightly greater tumor uptake initially compared to animals breathing air; however, after 27 min this difference was diminished. For animals breathing 100% oxygen, the tumor uptake was 48% less than that observed in air breathing animals 27 min post-injection. In contrast, Yuan *et al* have shown that carbogen breathing, which oxygenated the rat FSA tumor as validated by the EF5 hypoxia probe, did not decrease ^{64}Cu-ATSM tumor uptake (compared to air breathing animals) (31). Interestingly, in this study a direct comparison of tumor hypoxia was made comparing the hypoxia probe EF5 and ^{64}Cu-ATSM PET tumor binding for three rat tumor models. While a correlation with respect to hypoxia levels between EF5 and ^{64}Cu-ATSM was observed for two tumors, one tumor (FSA) showed no correlation at all, thus questioning the selectivity of ^{64}Cu-ATSM as a universal hypoxia marker (31). Consistent with this study, Burgman *et al*, found that ^{64}Cu-ATSM uptake *in vitro* was cell line-dependent, suggesting that ^{64}Cu-ATSM may be disease site specific (32). Interestingly, in this study one of the cell lines exhibited significant ^{64}Cu-ATSM uptake under aerobic conditions. Lastly, O'Donoghue *et al*, compared PET hypoxia imaging in two different rat tumor models for ^{64}Cu-ATSM and ^{18}F-FMiso and correlated the findings with oxygen electrode measurements (14). ^{18}F-FMiso scans taken over the first 1-4 h post-injection were relatively constant and generally agreed with electrode measurements for both tumors studied. However, for the R-3327 tumor ^{64}Cu-ATSM uptake was unstable over this time period and only when ^{64}Cu-ATSM tumor uptake scans were evaluated 16-20 h post-injection did they agree with the ^{18}F-FMiso/electrode data. For the other tumor (FaDu) both early and late ^{64}Cu-ATSM scans were similar and in general in agreement with the ^{18}F-FMiso/electrode data, demonstrating differences among tumor types with respect to ^{64}Cu-ATSM specificity for hypoxia imaging.

Additional studies were conducted using nitroimidazole binding (^{18}F-FMiso) in tumors in mice subjected to gases with different oxygen content. ^{18}F-FMiso tumor uptake was clearly different when compared to ^{64}Cu-ATSM uptake. ^{64}Cu-ATSM uptake was more uniform across the tumor; whereas, ^{18}F-FMiso uptake was more heterogeneous and spotty. While no statistical difference was demonstrated for the three oxygen breathing conditions, there was a trend for increased ^{18}F-FMiso tumor uptake (10% oxygen > air > carbogen).

As mentioned above, we have had experience in measuring oxygen levels in the SCCVII tumor for animals breathing air and carbogen using oxygen electrodes and have shown that carbogen markedly increases the oxygenation of SCCVII tumors (20). However, for the present study we included an independent assessment of tumor hypoxia using pimonidazole. By using the various inspired oxygen concentrations, the extent of hypoxia varied in the SCCVII tumor as evidenced by the pimonidazole hypoxia index values (Fig. 9). Carbogen breathing decreased hypoxia and 10% oxygen breathing clearly increased hypoxia in the SCCVII tumor, as expected.

In conclusion, with the SCCVII tumor model we were unable to demonstrate predictable changes in ^{64}Cu-ATSM tumor uptake when the oxygenation status of the tumor was modulated. Results using ^{18}F-FMiso were more positive with a trend toward greater uptake as hypoxia was increased in the tumor. The results of the present study question the use of ^{64}Cu-ATSM as a hypoxia specific marker; however, the avidity tumor uptake of ^{64}Cu-ATSM affords the opportunity of further research to discern the mechanism(s) of tumor binding.

Acknowledgments

This study was supported by the Intramural Research Program of the Center for Cancer Research, National Cancer Institute, NIH.

References

1. Teicher BA, Lazo JS and Sartorelli AC: Classification of antineoplastic agents by their selective toxicities toward oxygenated and hypoxic tumor cells. Cancer Res 41: 73-81, 1981.
2. Hockel M, Schlenger K, Aral B, Mitze M, Schaffer U and Vaupel P: Association between tumor hypoxia and malignant progression in advanced cancer of the uterine cervix. Cancer Res 56: 4509-4515, 1996.
3. Nordsmark M, Overgaard M and Overgaard J: Pretreatment oxygenation predicts radiation response in advanced squamous cell carcinoma of the head and neck. Radiother Oncol 41: 31-39, 1996.
4. Brizel DM, Sibley GS, Prosnitz LR, Scher RL and Dewhirst MW: Tumor hypoxia adversely affects the prognosis of carcinoma of the head and neck. Int J Radiat Oncol Biol Phys 38: 285-289, 1997.
5. Movsas B, Chapman JD, Hanlon AL, Horwitz EM, Greenberg RE, Stobbe C, Hanks GE and Pollack A: Hypoxic prostate/muscle pO_2 ratio predicts for biochemical failure in patients with prostate cancer: preliminary findings. Urology 60: 634-639, 2002.
6. Brown JM: Tumor microenvironment and the response to anticancer therapy. Cancer Biol Ther 1: 453-458, 2002.
7. Chapman JD, Engelhardt EL, Stobbe CC, Schneider RF and Hanks GE: Measuring hypoxia and predicting tumor radioresistance with nuclear medicine assays. Radiother Oncol 46: 229-237, 1998.
8. Chapman JD, Schneider RF, Urbain JL and Hanks GE: Single-photon emission computed tomography and positron-emission tomography assays for tissue oxygenation. Semin Radiat Oncol 11: 47-57, 2001.
9. Eschmann SM, Paulsen F, Reimold M, Dittmann H, Welz S, Reischl G, Machulla HJ and Bares R: Prognostic impact of hypoxia imaging with ^{18}F-misonidazole PET in non-small cell lung cancer and head and neck cancer before radiotherapy. J Nucl Med 46: 253-260, 2005.
10. Lewis JS, McCarthy DW, McCarthy TJ, Fujibayashi Y and Welch MJ: Evaluation of ^{64}Cu-ATSM *in vitro* and *in vivo* in a hypoxic tumor model. J Nucl Med 40: 177-183, 1999.
11. Lewis J, Laforest R, Buettner T, Song S, Fujibayashi Y, Connett J and Welch M: Copper-64-diacetyl-bis(N4-methylthiosemicarbazone): an agent for radiotherapy. Proc Natl Acad Sci USA 98: 1206-1211, 2001.
12. Dehdashti F, Grigsby PW, Mintun MA, Lewis JS, Siegel BA and Welch MJ: Assessing tumor hypoxia in cervical cancer by positron emission tomography with 60Cu-ATSM: relationship to therapeutic response-a preliminary report. Int J Radiat Oncol Biol Phys 55: 1233-1238, 2003.
13. Dehdashti F, Mintun MA, Lewis JS, Bradley J, Govindan R, Laforest R, Welch MJ and Siegel BA: *In vivo* assessment of tumor hypoxia in lung cancer with ^{60}Cu-ATSM. Eur J Nucl Med Mol Imaging 30: 844-850, 2003.
14. O'Donoghue JA, Zanzonico P, Pugachev A, Wen B, Smith-Jones P, Cai S, Burnazi E, Finn RD, Burgman P, Ruan S, Lewis JS, Welch MJ, Ling CC and Humm JL: Assessment of regional tumor hypoxia using (18)F-fluoromisonidazole and (64)Cu(II)-diacetyl-bis(N4-methylthiosemicarbazone) positron emission tomography: comparative study featuring microPET imaging, Po(2) probe measurement, autoradiography, and fluorescent microscopy in the R3327-AT and FaDu rat tumor models. Int J Radiat Oncol Biol Phys 61: 1493-1502, 2005.
15. Fujibayashi Y, Taniuchi H, Yonekura Y, Ohtani H, Konishi J and Yokoyama A: Copper-62-ATSM: a new hypoxia imaging agent with high membrane permeability and low redox potential. J Nucl Med 38: 1155-1160, 1997.
16. Maurer RI, Blower PJ, Dilworth JR, Reynolds CA, Zheng Y and Mullen GE: Studies on the mechanism of hypoxic selectivity in copper bis(thiosemicarbazone) radiopharmaceuticals. J Med Chem 45: 1420-1431, 2002.
17. Aft RL, Lewis JS, Zhang F, Kim J and Welch MJ: Enhancing targeted radiotherapy by copper(II)diacetyl- bis(N4-methylthiosemicarbazone) using 2-deoxy-D-glucose. Cancer Res 63: 5496-5504, 2003.
18. Rajendran JG, Wilson DC, Conrad EU, Peterson LM, Bruckner JD, Rasey JS, Chin LK, Hofstrand PD, Grierson JR, Eary JF and Krohn KA: [(18)F]FMISO and [(18)F]FDG PET imaging in soft tissue sarcomas: correlation of hypoxia, metabolism and VEGF expression. Eur J Nucl Med Mol Imaging 30: 695-704, 2003.
19. Koch CJ and Evans SM: Non-invasive PET and SPECT imaging of tissue hypoxia using isotopically labeled 2-nitroimidazoles. Adv Exp Med Biol 510: 285-292, 2003.
20. Krishna MC, English S, Yamada K, Yoo J, Murugesan R, Devasahayam N, Cook JA, Golman K, Ardenkjaer-Larsen JH, Subramanian S and Mitchell JB: Overhauser enhanced magnetic resonance imaging for tumor oximetry: coregistration of tumor anatomy and tissue oxygen concentration. Proc Natl Acad Sci USA 99: 2216-2221, 2002.
21. Szajek LP, Kao C-HK, Kiesewetter DO, Sassaman MB, Lang L, Plascjak P and Eckelman WC: Semi-remote production of [^{64}Cu]$CuCl_2$ and preparation of high specific activity [^{64}Cu]Cu-ATSM for PET studies. Radiochim Acta 93: 239-244, 2005.
22. Obata A, Yoshimoto M, Kasamatsu S, Naiki H, Takamatsu S, Kashikura K, Furukawa T, Lewis JS, Welch MJ, Saji H, Yonekura Y and Fujibayashi Y: Intra-tumoral distribution of (64)Cu-ATSM: a comparison study with FDG. Nucl Med Biol 30: 529-534, 2003.
23. Sorger D, Patt M, Kumar P, Wiebe LI, Barthel H, Seese A, Dannenberg C, Tannapfel A, Kluge R and Sabri O: [^{18}F]Fluoroazomycinarabinofuranoside (18FAZA) and [^{18}F]Fluoromisonidazole (^{18}FMISO): a comparative study of their selective uptake in hypoxic cells and PET imaging in experimental rat tumors. Nucl Med Biol 30: 317-326, 2003.
24. Seidel J, Vaquero J and Green MV: Resolution uniformity and sensitivity of the NIH ATLAS small animal PET scanner. Nucl Sci Symp Conf Rec, IEEE 3: 1555-1558, 2001.
25. Seidel J, Vaquero J, Pascau J, Desco M, Johnson CA and Green MV: Features of the NIH ATLAS small animal PET scanner and its use with a coaxial small animal volume CT scanner. Biomed Imag Biol 4: 545-548, 2002.

26. Seidel J, Vaquero JJ and Green MV: Resolution uniformity and sensitivity of the NIH ATLAS small animal PET scanner: comparison to simulated LSO scanners without depth-of-interaction capability. IEEE Trans Nucl Sci 50: 1347-1350, 2003.
27. Johnson CA, Seidel J, Carson RE, Gandler WR, Sofer A, Green MV and Daube-Witherspoon ME: Evaluation of 3D reconstruction algorithms for a small animal PET camera. IEEE Trans Nucl Sci 44: 1303-1308, 1997.
28. Raleigh JA, Chou SC, Arteel GE and Horsman MR: Comparisons among pimonidazole binding, oxygen electrode measurements, and radiation response in C3H mouse tumors. Radiat Res 151: 580-589, 1999.
29. Lewis JS, Sharp TL, Laforest R, Fujibayashi Y and Welch MJ: Tumor uptake of copper-diacetyl-bis[N(4)-methylthiosemicarbazone]: effect of changes in tissue oxygenation. J Nucl Med 42: 655-661, 2001.
30. Obata A, Kasamatsu S, Lewis JS, Furukawa T, Takamatsu S, Toyohara J, Asai T, Welch MJ, Adams SG, Saji H, Yonekura Y and Fujibayashi Y: Basic characterization of ^{64}Cu-ATSM as a radiotherapy agent. Nucl Med Biol 32: 21-28, 2005.
31. Yuan H, Schroeder T, Bowsher JE, Hedlund LW, Wong T and Dewhirst MW: Inter-tumoral differences in hypoxia selectivity of the PET imaging agent (64)CuII-diacetyl-bis(N4-methylthiosemicarbazone). J Nucl Med 47: 989-998, 2006.
32. Burgman P, O'Donoghue JA, Lewis JS, Welch MJ, Humm JL and Ling CC: Cell line-dependent differences in uptake and retention of the hypoxia-selective nuclear imaging agent Cu-ATSM. Nucl Med Biol 32: 623-630, 2005.